Development of CMC Heat Exchanger and Its Thermo-fluid Dynamics Performance

Toyoaki YOSHIDA[1], Takao KUMAGAI[1] and Takashi YAMANE[1]

[1]Aaeronautical Environment Technology Center
Institute of Space Technology and Aeronautics, Japan Aerospace Exploration Agency
7-44-1 Jindaiji-higashi, Chofu, Tokyo 182-8522, JAPAN
Phone: +81-422-40-3416, Fax: +81-422-40-3429, E-mail: yoshida.toyoaki@jaxa.jp

ABSTRACT

The aim of the present research is to provide some constructive technical information on lightweight and high-temperature heat exchangers for future regenerative gas turbines. The authors have concentrated on seeking application of advanced ceramic materials and heat transfer construction suitable for compact heat exchangers. The resulting test model introduced in the study was the type of corrugated straight fins with a flat plate made of SiC-SiC composite (Ceramic Matrix Ceramic) by the chemical vapor infiltration (CVI) method.

Trial manufactures of the above model and its mechanical strength evaluations were conducted. Heat transfer tests have been performed in a high-temperature wind tunnel at NAL. From the obtained experimental data, the effects of Reynolds number, temperature ratio and gas temperature on friction coefficient, Nusselt number and heat exchanger effectiveness were surveyed. Also these heat transfer and pressure loss characteristics were compared with those of published data that had been obtained for metal heat exchangers with similar constructions to the present one, such as pin fin pedestals and corrugated straight fins. As general trends, the results from the present heat exchanger, heat transfer coefficients and pressure loss coefficients, showed lower than those of the pin fin pedestal type, while showed higher than those of the corrugated straight fins metal heat exchanger.

Additionally, a trial numerical simulation has also been performed in order to see the heat and flow around the heat exchanger component, by applying a conjugate analysis program package for fluid flow around a solid body and heat conduction in the body that was recently developed by one of the authors.

NOMENCLATURE

A cross-section area of a fin [mm^2] (Fig.4)
d_e reference diameter of a fin [m, mm] (Fig.4)
f Fanning's friction coefficient, Eq.(1) [-]
G mass flow rate per one plate [kg/s] (Table 1)
h heat transfer coefficient [W/(m^{2}K)]
L length of a straight fin [m, mm] (Fig.4)
L_f $2L_f$: height of a straight fin [mm] (Fig.4)
Nu Nusselt number =$h \cdot d_e / \lambda$, [-]
P pressure [Pa]
P_f width of a fin [mm] (Fig.4)
Pr Prandtl number [-]
Q thermal energy [kW] (Fig.8)
R relative aspect ratio =$2L_f/(2L_f+P_f)$, [-]
Re Reynolds number =$u_m d_e \rho / \mu$, [-]
T temperature [K, deg.C]

t_b thickness of a plate [mm] (Fig.4)
u_m mean velocity of flow [m/s]
β mass flow rate ratio [-] (Table 1)
ΔP total pressure difference =$P_{in}-P_{out}$, [Pa]
λ thermal conductivity [W/(mK)]
μ viscosity [Pa·s]
ρ density [kg/m^3]
ϕ thermal effectiveness, Eq.(2) [-]

Subscripts
ave average
in inlet
out outlet
1 hot gas side
2 cold air side

INTRODUCTION

High temperature heat exchangers have been necessitated and developed in many industrial fields. As to gas turbine heat exchangers, working gas temperature has been increasing for the improvement of thermal efficiency through the elevation of turbine inlet temperature. Since 1980s research and development of ceramic heat exchangers have been evolved under the advancement in manufacturing technology of high-temperature ceramic materials such as silicon nitride (Si_3N_4), silicon carbide (SiC) and those composite materials (Avran and Boudigues, 1987, and Ito, 1990).

Compared to superalloys, the above ceramics have far lighter specific density (3.1-3.2) and far higher temperature durability (say, 200K or even higher). Hence if one can apply the above ceramics to heat exchangers, significant advancements in thermal efficiency, size and weight can be attained. In general, the major subjects for the development of ceramic heat exchangers are the following two points. (1) Manufacturing technology of relatively big parts (say, larger than 50cm in length) with high heat transfer configuration. (2) To establish a satisfying seal mechanism at the interface between the ceramic parts and those surrounding metal parts. Since these subjects have been very difficult problems to be overcome, metal heat exchangers have extensively been applied even in high-temperature region up to 1150K level using nickel-base superalloys.

The present study was motivated by the above mentioned situation and the following hopeful view of SiC. Its flexural strength can be an order of 400MPa and keeps unchanged up to very high temperature, 1670K. Hence the authors have been engaged in development of a high-temperature ceramic heat exchanger element made of SiC-SiC ceramic matrix composite in collaboration with the Mitsui Engineering & Shipbuilding Co., Ltd.

(Matsumoto and Fujioka, 1996). Construction of the heat exchanger element is composed of corrugated straight fins and a flat plate. This paper introduces trial manufactures of the element and evaluations of its mechanical strength at first. Experimental heat transfer and flow analyses of the heat exchanger model are described as the main body. Lastly, detailed temperature fields in a set of the unit straight passage of the hot gas side and the cold air side element are introduced by a set of results from the numerical simulation applying a conjugate analysis program.

CMC HEAT EXCHANGER

The heat exchanger element introduced in the present study was the type of corrugated straight fins with a flat plate both made of SiC-SiC composite. SiC fiber raw materials for both constructions were woven in one body. Chemical vapor infiltration (CVI) of SiC was then applied to the element. The rectangular and flat eleven elements were piled alternatively, forming a cross-flow type heat exchanger. Fig.1 shows a schematic construction of the present heat exchanger test model. Fig.2 shows a general view of the actual test model under its assembly. The frame of the heat exchanger was made of carbon ceramics. Spacers made of the same material and ceramic adhesive seal material (seen in white color) were used for the assembly of the test body. Thermocouple leading wires for gas and wall temperature measurements are also seen in the figure.

Fig.3 shows a general view of a single element before its assembly. Since the element is woven with SiC fibers, the disposition of the surface is uneven depending on the size of fibers. This may contribute for augmentation of heat transfer to some extent. In this figure, a pair of spacers is photographed together. Also the locations of temperature measurement and situation of thermocouple leading wires can be seen. Heat transfer coefficients were calculated with gas and wall temperatures by these thermocouples and thermal energies transferred in cold air and hot gas flow, respectively. Detailed dimensions of the corrugated straight fins and the plate are given in Fig.4. These were measured for the completed test model element.

After the CVI process was done, the element plate was a bit curved due to the course of high temperature reaction. Since the compactness of fiber cloth is relatively coarse in the part of the fins, the cloth is permeated by air even after the CVI, while in the part of bottom plate, the cloth becomes impermeable because of its high density. Pressure-proof tests were performed with the completed heat exchanger elements by using compressed air. As a result, it was found that the element could bear air pressure up to 250kPa. As for its temperature durability, it is already known that CMC of SiC-SiC can bear temperature up to an order of 1573K.

The flatness of the element plate and sealing of working gas flows at the element ends were realized during the assembly. The eleven elements were suppressed with top and bottom plates and these plates were fastened by carbon ceramic screws at the four corners of the plates.

HEAT TRANSFER EXPERIMENTS

Heat transfer and pressure loss characteristics of the present heat exchanger have been investigated in a high-temperature wind tunnel at NAL. Fig.5 shows a schematic system of the wind tunnel. The heat exchanger test model was placed in the test section. Since the present heat exchanger was intended for regenerative gas turbine applications, mass flow rate of hot gas flow was kept almost the same as that of cold air flow in a series of the experiments . A cooler in the hot gas side and a heater in the cold air side were used to vary and adjust temperature ratio.

Experimental conditions are shown in Table 1. Numerals in the respective parenthesis denote the highest and the lowest deviations from a designated value. Parameters chosen in the present study were Reynolds numbers and gas temperatures both in hot gas flow and cold air flow, and temperature ratio of the gas to the air flows.

Before the heat transfer tests were performed, temperature and pressure distributions of the hot gas flow were measured at the inlet of the test section. The results are given in Fig.6 (total temperature) and Fig.7 (total pressure), respectively. When the fuel was burned in the combustor, the total temperature showed its maximum value around the center of the flow passage and gradually decreased toward the top and bottom walls. The deviation between the maximum and the averaged value was 4.45% for $T_{1in,ave}$=368.0 deg.C, and 5.90% for $T_{1in,ave}$=649.2 deg.C, respectively. On the other hand, when the main flow was not burned, the total temperature distribution showed almost uniform. As for the total pressure, its variation was not uniform and seemed stay almost constant within the range of accuracy of the pressure measurement system. In fact, the maximum deviation was less than 0.44%. Notes that three kinds of symbols in Fig.6 and Fig.7 stand for the same experimental conditions, respectively.

During the heat transfer performance tests, total temperature and pressure at each cross-section, such as inlet and outlet sections of the main gas flow and the cold air flow, were measured with a one point temperature and pressure probe, respectively. The respective probe was situated at the center of the each cross-section. Only the inlet main flow total temperature was corrected to average value with the use of the relation between the maximum and the average values as given in Fig.6. The other measured values were considered as average values within the range of uncertainties.

Fig.8 shows a result example of heat transfer rate evaluations in the whole domain of the experiments. The total thermal energy generated at the combustor was an order of 130kW. 85～89% of the total energy was preserved in the exit gas flow. Only 6～8% was transferred to the cold air flow and almost the same order of heat was released to the ambient air as a heat loss. This comes mainly from the fact that the present test model is relatively too small as a complete heat exchanger and can only be a partial model, or an element. This is due to size restrictions existed in processing facilities for the chemical vapor infiltration.

Hence the heat exchanger effectiveness (thermal effectiveness) obtained from the present experiments remains considerably small. It may not be appropriate to evaluate the present data as that of a complete unit of a heat exchanger. Even so, we can discuss its characteristics under the influence of affecting factors such as Reynolds number, temperature ratio and gas temperature. Furthermore, we can discuss heat transfer (Nusselt number) and pressure loss characteristics for the corrugated straight fins construction.

EXPERIMETNAL RESULTS AND DISCUSSION

The construction of the present heat exchanger is a type of corrugated straight fins with a flat plate. It is not a new and special construction but rather conventional one. The originality is that it was made of fiber cloth of SiC ceramics and CVI was applied to the element. Compared to the current metal heat exchangers with similar construction, the surface condition is wavy and rough. This may cause different aerodynamic and heat transfer performances from those of the existing ones. Hence the present results are compared with those from the metal heat exchanger having very similar configuration (Fujikake, 1977, and Kays and London, 1964). The comparisons are also done with performances of short pin fins type (VanFossen, 1981, and Metzger and Haley, 1982) and tube banks type (Fujii and Niizato, 1985, and Jacob, 1938) of heat exchanger constructions.

Aerodynamic Performance (Friction Coefficient)

For aerodynamic performance of heat exchangers, Fanning's friction coefficient is often used and it is defined as follows.

$$f = (d_e / 2\rho u_m^2)(\Delta P / L) \qquad (1)$$

For the discussion of pressure loss characteristics among various types of construction, a pressure loss normalized by kinetic energy of mean flow, "f·L/d$_e$" is usually introduced.

Pressure loss characteristics with respect to Reynolds number from the experiment S (see Table 1) are shown in Fig.9 and Figs.10 (a) and (b). The present friction coefficients, "f"s are located below 0.01 and most "f·L/d$_e$"s are located between 0.3 and 0.4 within the experimental range of cold air flow Reynolds number. As shown in Fig.9, dimensionless pressure losses of the present heat exchanger are considerably lower than those of the short pin fins (Metzger and Haley, 1982) and the tube banks (Fujii and Niizato, 1985, and Jacob, 1938). On the other hand, we can see in Figs.10 (a) and (b) that they are larger than those of the corrugated straight fins (Fujikake, 1977, and Kays and London, 1964). This may come from the differences of surface condition and the length, L between the present case and the referred cases. The present heat exchanger element has rough and wavy surface, while the others are smooth because they are made with metal sheets. The present "L/d$_e$"s are 37.3 and 41.4 (see Fig.4), while the others are 7.7, 9.0, 10.3 and 24.7, respectively.

When both the hot gas flow Reynolds number, Re$_1$ and the cold air flow Reynolds number, Re$_2$ are fixed, the pressure loss characteristics remain unchanged against temperature ratio as shown in Fig.11. Further, under a constant temperature ratio, the inlet gas temperature, T$_{1in}$ has little influence on the pressure loss as shown in Fig.12.

Heat Transfer Characteristics (Nusselt Number)

The experimental results are given from Fig.13 through Fig.16. The effect of Reynolds number on Nusselt number are shown in Fig.13, Figs.14 (a) and (b) in comparisons with works referred in the previous section. A general trend of the present results, a gradient of the data fitted curve, is almost the same as those of the cited works. Consistent with the results of pressure loss characteristics, the present Nusselt numbers are located lower than those of the short pin fins (Metzger and Haley, 1982, and VanFossen, 1981). However the two curves are closer each other than the corresponding results obtained for pressure loss characteristics (Fig.9). It is necessary to note that the reference length in Reynolds number is a pin fin diameter in Metzger and Haley's work and a hydraulic diameter in VanFossen's work, respectively. In comparison of the results among existing corrugated straight fins (Fig.14 (a) and (b)), the present results are located higher than those of earlier works (Fujikake, 1977, and Kays and London, 1964). This is again consistent with the results of pressure loss characteristics. Hence, the reasons for the trend of Nusselt number results may be the same as those for the pressure loss characteristics.

When both Re$_1$ and Re$_2$ are fixed, Nusselt number tends to increase gradually with respect to temperature ratio as shown in Fig.15. Furthermore, even under a constant temperature ratio, Nusselt number increases with increasing inlet gas temperature as shown in Fig.16. These are different with the facts for the pressure loss characteristics. This may come from the nature that physical properties such as thermal conductivity and so on depend on temperature.

Heat Exchanger Effectiveness (Thermal Effectiveness)

Thermal effectiveness is a very important performance index for evaluations of heat exchangers. It is defined as follows.

$$\phi = (T_{2out} - T_{2in})/(T_{1in} - T_{2in}) \qquad (2)$$

As already described in the previous chapter, the present test model is relatively too small as a complete heat exchanger. Hence absolute values of the thermal effectiveness obtained from the experiments can only be reference data. However the discussion of its trend with respect to affecting factors is very valuable for general applications.

Fig.17 shows a general trend of thermal effectiveness, ϕ in connection with the Reynolds number of cold air flow. Absolute values of ϕ are situated around 0.1 and have a slightly descending slope with increasing Reynolds number. On the other hand, as shown in Fig.18, ϕ s gradually increase and reach a certain constant value with increasing temperature ratio. According to Fig.19, thermal effectiveness, ϕ apparently increases with respect to hot gas temperature under a constant temperature ratio. This may also come from the temperature dependence of physical properties that exert influence on heat transfer rate, namely temperature variations both in the hot gas side and the cold air side.

UNCERTAINTIES IN THE EXPERIMENTS

Fundamental uncertainties in temperature and pressure measurements are 1deg.C and 1kPa, respectively. In Table 1, average values of the experimental conditions are given together with those highest and lowest deviations. From these variations contained in raw data and processed data, resulting relative errors of major variables are estimated as follows,

(df/f)$_{max}$=20.7%, (d(Nu)/Nu)$_{max}$=28.2%, and (dϕ/ϕ)$_{max}$=16.2%.

CONJUGATE ANALYSIS OF HEAT AND FLOW IN THE FLOW PASSAGES

One of the authors has been engaged in development of a common CFD platform called UPACS (Yamane and others, 2000). The UPACS deals with CFD around a complete system such as an aircraft and a jet engine. Recently, a conjugate analysis of heat and flow around and in a solid body has been completed and added to the UPACS by Yamane and others (2003). Here a trial execution of the conjugate analysis has been done to the present heat exchanger. Figures 20 and 21 show the results of temperature fields in and around the heat exchanger element under a typical experimental condition, T$_{1in}$=328.2 deg.C, P$_{t1in}$=0.18258 MPa, T$_{2in}$=131.6 deg.C, P$_{t2in}$=0.18331 MPa, β =1.023.

Since these results are from initial and trial computations, and various considerations of validation in the simulation by comparisons with experimental results are not given yet, quantitative agreement between numerical and experimental data is not enough. However a general trend of temperature fields are considered very appropriate both in the plate (Fig.20) and in the flow passages (Fig.21). One can see detailed temperature and flow variations in and around the heat exchanger element by this kind of numerical work. Hence after enough improvement of the present numerical procedure, these simulations will be very effective for the design and improvement of heat exchangers in the future.

CONCLUDING REMARKS

A heat exchanger element with corrugated straight fins was successfully manufactured by the application of chemical vapor infiltration to SiC-SiC ceramic matrix ceramic composite. The major results obtained from the present study are as follows.

The heat exchanger element can bear pressure difference up to 250kPa and temperature level up to 1573K.

As to aerodynamic performances, friction coefficients of the present construction are considerably lower than those of the short pin fins and the tube banks. On the other hand, they are larger than those of the corrugated straight fins made with metal sheets because of the rough surface condition in the present case. The present friction coefficients remain almost constant under varying temperature ratio and gas temperature when the rest of parameters such as Reynolds number are kept unchanged.

Heat transfer performances are consistent with the above comparisons. That is, the present Nusselt numbers are located lower than those of the short pin fins, while they are higher than those of the corrugated straight fins made with metal sheets. Different from the friction coefficients, heat transfer characteristics receive influences from the temperature conditions. Nusselt number tends to increase with respect of temperature ratio and gas temperature itself because the physical properties have temperature dependence.

The present thermal effectiveness shows slight decrease with increasing Reynolds number. It gradually increases and reaches a certain constant value with increasing temperature ratio. And it apparently increases with respect to hot gas temperature.

The numerical simulation applying a conjugate analysis of heat and flow around and in the heat exchanger element can be a very effective tool for the design and improvement of the heat exchangers in the future.

REFERENCES

Avran, P. and Boudigues, S., 1987, Ceramic Turbine Blades and Heat Exchangers Theory and Experimental Results, *Proceedings, 87-Tokyo-IGTC,* pp.I-163-168.

Fujii, T. and Niizato, K., 1985, Consideration on Estimating Method for Flow Resistance Coefficient in Tube Banks, *Bulletin of the JSME, B,* Vol.51, No.461, pp.356-360.

Fujikake,K., 1977, Research on Corrugated Straight Fins Heat Exchanger, Part 2, *Bulletin of the JSME,* Vol.43 No.365, pp. 241-249.

Ito, M., 1990, Ceramic Heat Exchangers for High-temperature Use, *FC Report,* Vol.8, No5, pp.156-162.

Jacob, M., 1938, Heat Transfer and Flow Resistance on Cross Flow of Gases over Tube Banks, *Trans ASME,* Vol.59, pp.384-386.

Kays, W.A. and London, A.L., 1964, Compact Heat Exchanger, McGraw-Hill.

Matsumoto, K. and Fujioka, N., 1996, Properties at High Temperatures of Fiber-Reinforced SiC Composite, *Mitsui Zosen Technical Review,* Vol.157, pp.43-47.

Metzger, D.E. and Haley,S.W., 1982, Heat Transfer Experiments and Flow Visualization for Arrays of Short Pin Fins, *ASME GT paper,* 82-GT-138.

VanFossen, G.L., 1981, Heat Transfer Coefficients for Staggered Arrays of Short Pin Fins, *ASME GT paper,* 81-GT-75.

Yamane, T., Yamamoto, K., Enomoto, S., Yamazaki, H., Takagi, R. and Iwamiya, T., 2000, Development of a Common CFD Platform –UPACS-, *Proceedings of the Parallel CFD 2000 Conference,* pp.257-264.

Yamane, T., Mimura, F., Yoshida, T., Yamawaki, S., Nakamata, C. and Imai, R., 2003, Coupled Simulations of Flow and Heat Conduction for Turbine Cooling, *Proceedings of the International Gas Turbine Congress 2003, Tokyo.*
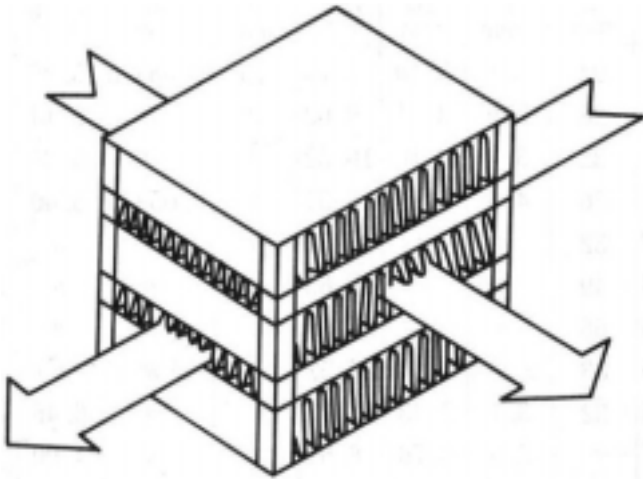
Fig.1 Schematic construction of the heat exchanger

Fig.2 General view of the heat transfer test model under its assembly
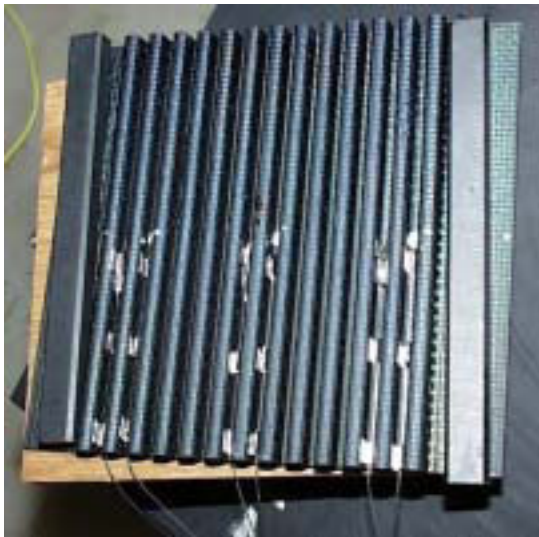
Fig.3 General view of the heat exchanger element
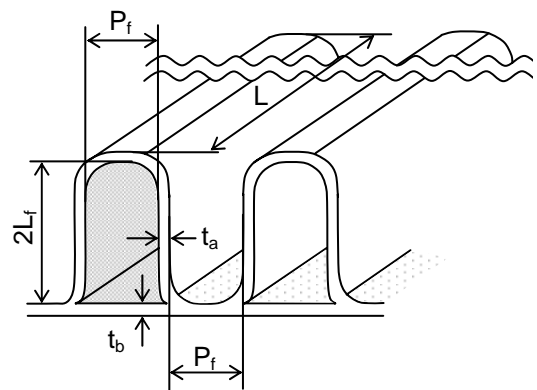
Passage cross-section
(hatched area)
$\left[\begin{array}{l} \text{Peripheral length}(L_p) : 22.27\text{mm} \\ \text{Cross-section area}(A) : 16.41\text{mm}^2 \\ \text{Reference diameter}(de) : 2.95\text{mm} \end{array}\right]$
        $=4A/L_p$
$2L_f : 5.78\text{mm}, P_f : 2.83\text{mm}$
$t_a : 0.62\text{mm}, t_b : 0.70\text{mm}$
L : 110mm (hot gas plate)
    122mm (cold air plate)

Fig.4 Dimension of the corrugated straight fins and a plate
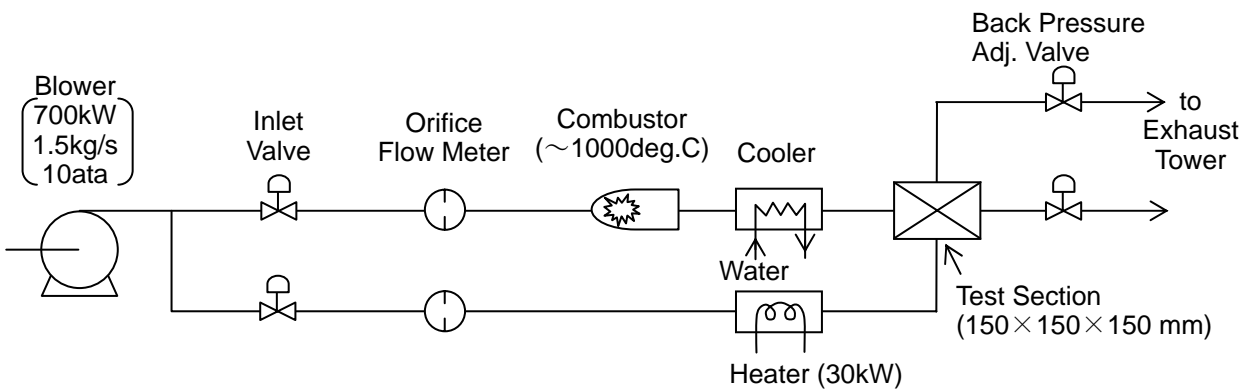
Fig.5 Schematic system of the wind tunnel for heat transfer tests

Table 1 Experimental conditions [Highest deviation / Lowest deviation]

Exp.Name	Re_1 $\times 10^4$	Re_2 $\times 10^4$	β	T_{1in} [deg.C]	T_{2in} [deg.C]	T_{1in}/T_{2in} [K／K]
S	1.4〜3.6	2.1〜5.4	1.001 (+0.006 / −0.011)	306.4 (+1.1 / −3.6)	128.5 (+3.1 / −7.6)	1.44 (+0.03 / −0.01)
T	2.77 (+0.03 / −0.05)	3.93 (+0.16 / −0.26)	1.004 (+0.011 / −0.008)	306.5 (+2.3 / −1.2)	132〜180	1.27〜1.43
U	1.58 (+0.02 / −0.01)	2.23 (+0.29 / −0.20)	1.006 (+0.006 / −0.006)	306.3 (+3.5 / −2.1)	97〜213	1.19〜1.56
V	1.60 (+0.03 / −0.03)	2.38 (+0.09 / −0.07)	1.001 (+0.007 / −0.013)	259〜506	84〜206	1.51 (+0.12 / −0.05)

Suffix 1 : Hot gas side, 2 : Cold air side

Re : Reynolds number at unit passage, $Re_1 = \rho_{1m} u_{1m} d_e / \mu_{1m}$, $Re_2 = \rho_{2m} u_{2m} d_e / \mu_{2m}$

β : mass flow rate ratio = G_1/G_2, G : mass flow rate per one plate
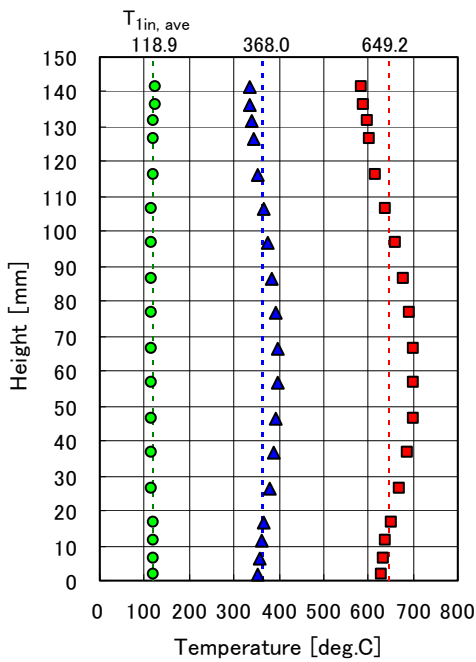
Fig.6 Total temperature distribution at the inlet of the main hot gas flow
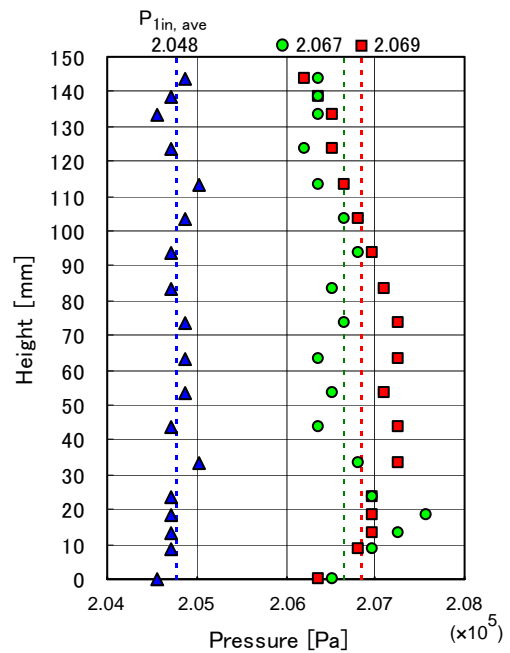
Fig.7 Total pressure distribution at the inlet of the main hot gas flow
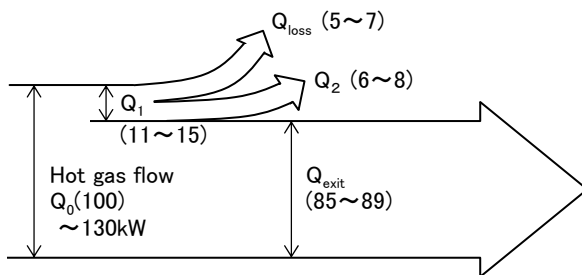
Q_0 : Total thermal energy generated at combustor
Q_1 : Thermal energy transfered to heat exchanger section
Q_2 : Thermal energy that cold air receives
Q_{loss} : Thermal energy discharged to environment
Q_{exit} : Thermal energy that exit flow preserves

Fig.8 Energy balance in the whole domain of the experiments
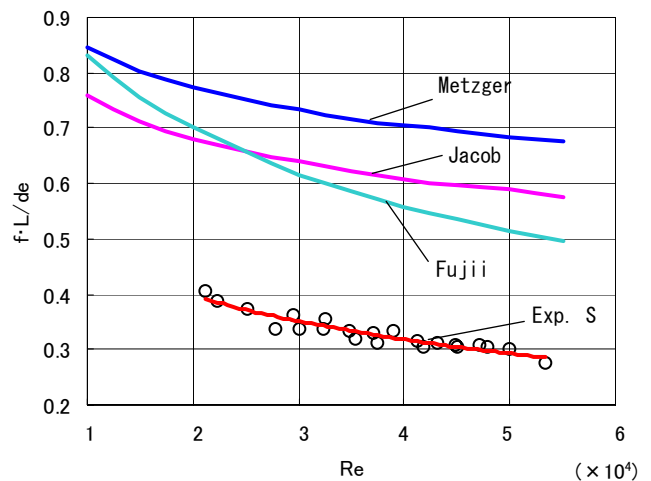
Fig.9 f・L/de versus Reynolds number
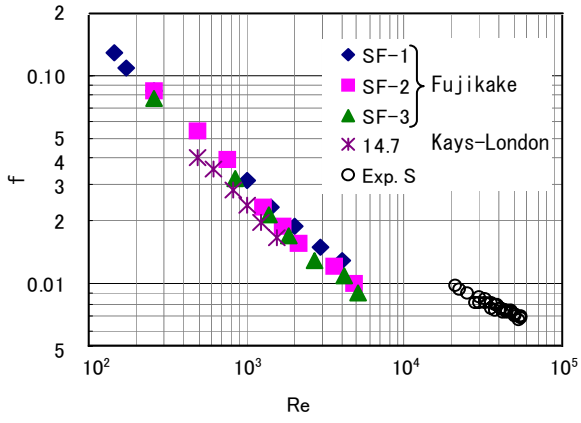
Fig.10 (a) Friction coefficient versus Reynolds number
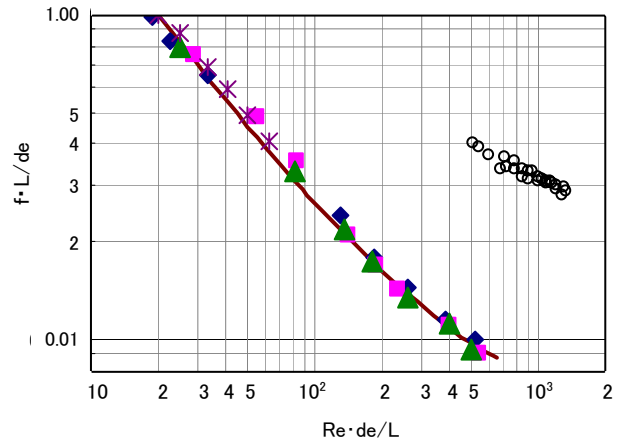
Fig.10 (b) f・L/de versus Re・de/L
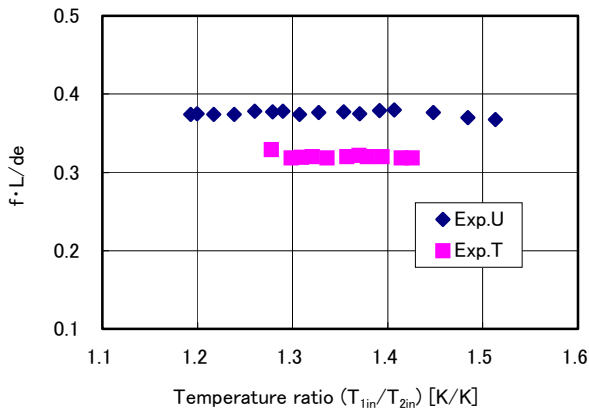
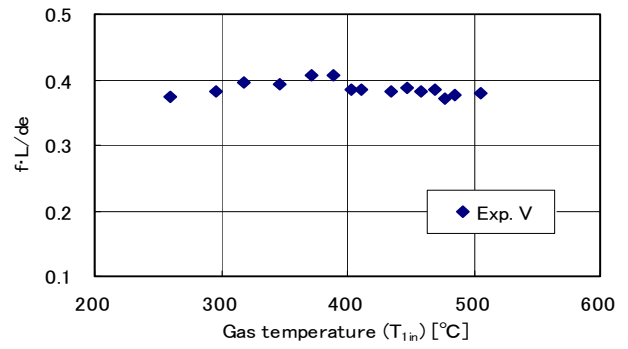Fig.11 Friction coefficient versus temperature ratio

Fig.12 Friction coefficient versus gas temperature

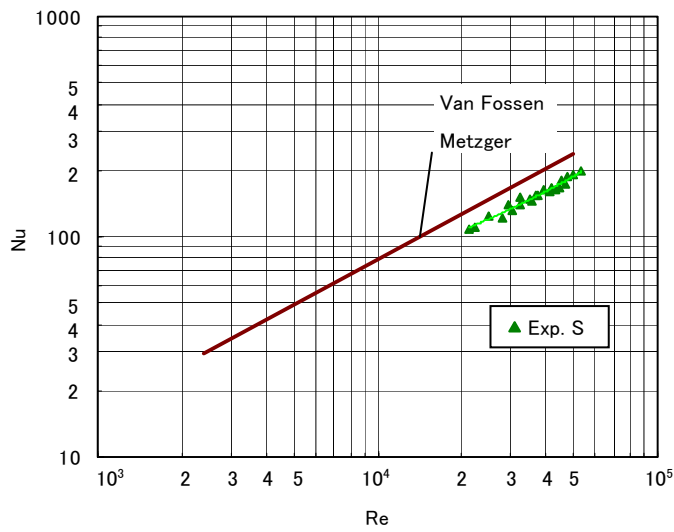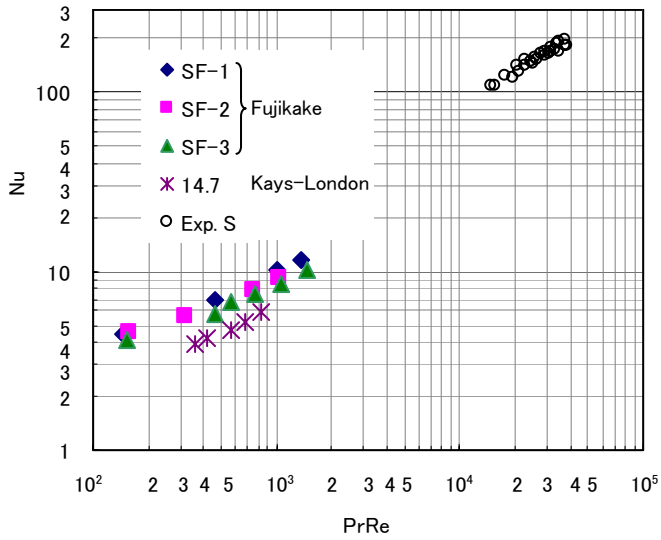Fig.13 Nusselt number versus Reynolds number

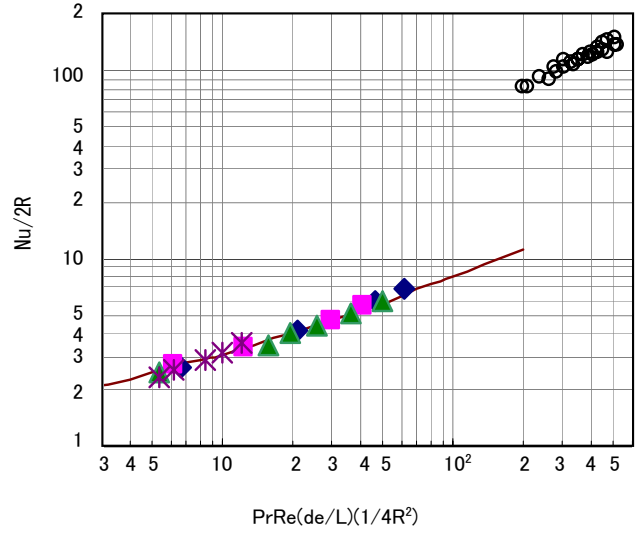Fig.14 (a) Nusselt number versus PrRe

Fig.14 (b) Nu/2R versus PrRe(de/L)(1/4R^2)

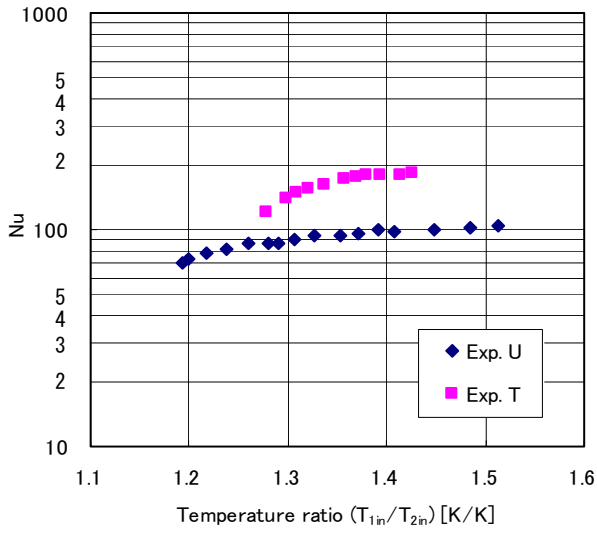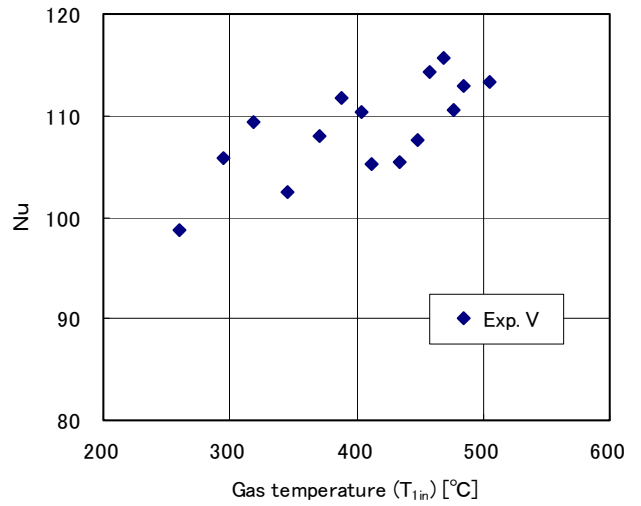Fig.15 Nusselt number versus temperature ratio
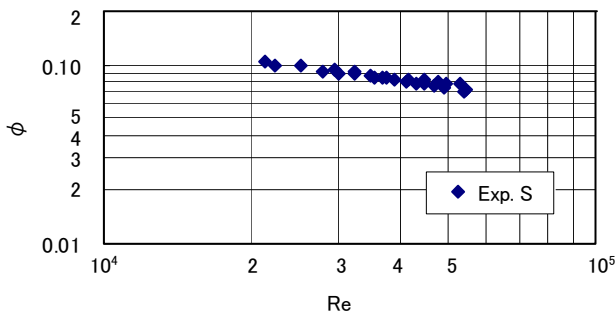

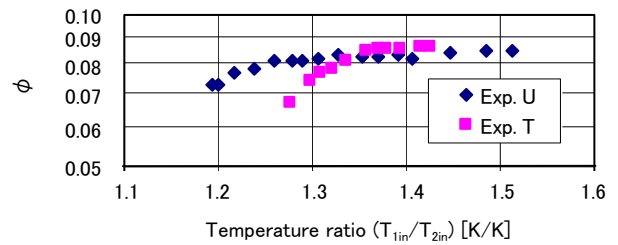Fig.16 Nusselt number versus gas temperature

Fig.17 Thermal effectiveness versus Reynolds number

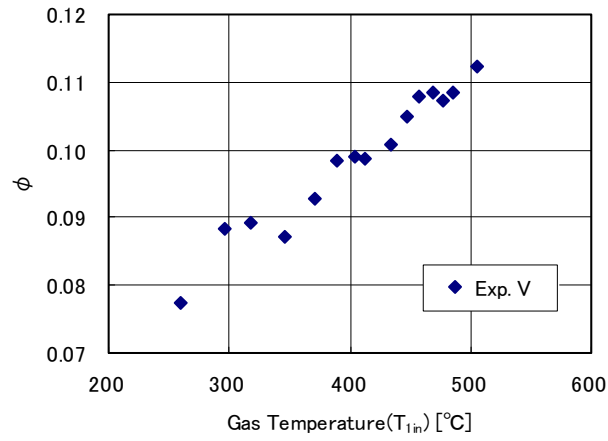Fig.18 Thermal effectiveness versus temperature ratio

Fig.19 Thermal effectiveness versus gas temperature
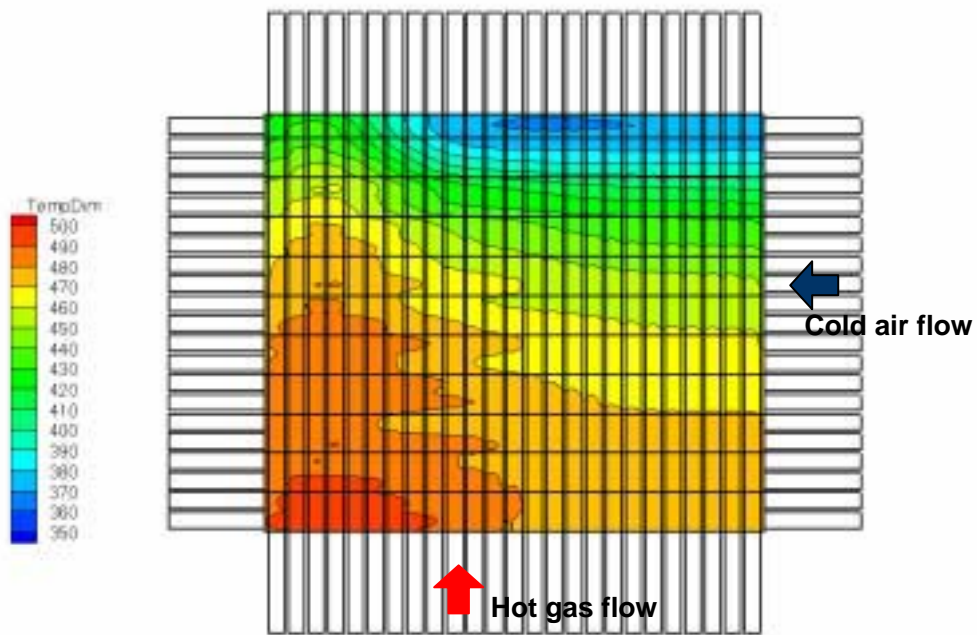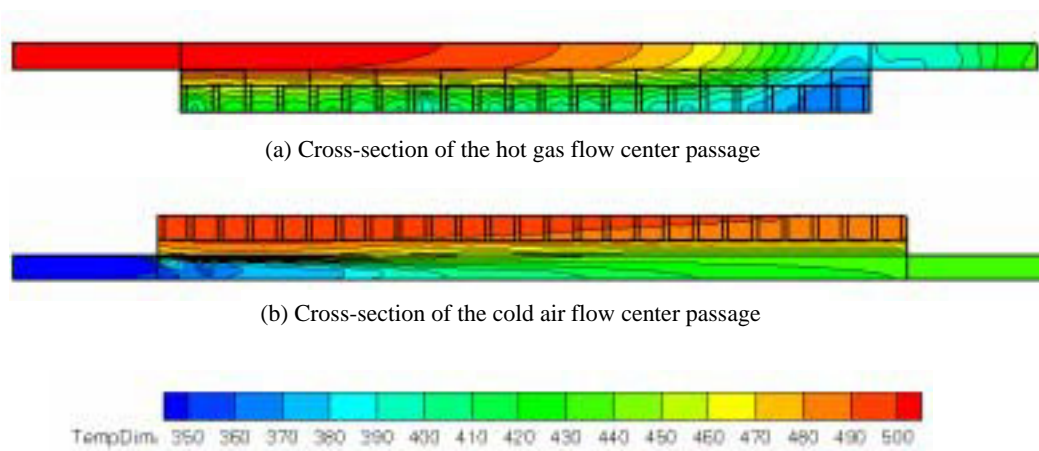

Cold air flow

Hot gas flow

Fig.20 Wall temperature distribution in the center plane of the element plate

(a) Cross-section of the hot gas flow center passage

(b) Cross-section of the cold air flow center passage

Fig.21 Temperature distributions in the center passages